

*Journal of*  
***Mechanics of***  
***Materials and Structures***

**QUASISTATIC DEFORMATION AND FAILURE MODES OF  
COMPOSITE SQUARE HONEYCOMBS**

Benjamin P. Russell, Vikram S. Deshpande and Haydn N. G. Wadley

***Volume 3, N° 7***

***September 2008***



## QUASISTATIC DEFORMATION AND FAILURE MODES OF COMPOSITE SQUARE HONEYCOMBS

BENJAMIN P. RUSSELL, VIKRAM S. DESHPANDE AND HAYDN N. G. WADLEY

Carbon fibre epoxy matrix composite honeycombs have been fabricated by slotting, assembling and adhesively bonding composite laminate sheets with various fibre architectures. Their out-of-plane compressive and in-plane shear responses were measured as a function of relative density, ratio of the cell height to width and the number of cells in the specimen. The measurements indicate that the response is relatively insensitive to the ratio of the cell height to cell width and number of cells in the specimen but is strongly dependent on the laminate type and fibre orientation. For example, the compressive strength of the honeycombs made from  $0 - 90^\circ$  laminates with fibres aligned with the compression direction was greater than that of honeycombs made from a woven material with fibres at  $\pm 45^\circ$ . However, the shear strengths exhibited the opposite trend. These differences were attributed to a change in failure mode. In compression the honeycombs failed by either elastic buckling or plastic microbuckling while in shear the two main failure modes were elastic buckling or shear failure of the composite sheet material. Analytical models are derived for these collapse modes and used to predict the strength of the honeycomb structure. The predicted strengths are substantially higher than the measurements due to the presence of manufacturing imperfections in the honeycombs that are not accounted for in the analytical models. A limited finite element (FE) investigation is also reported to quantify the effects of imperfections on the compressive strength of the composite honeycombs. The measurements and analytical predictions reported here indicate that composite cellular materials such as honeycombs reside in a gap in the strength versus density material property space, providing new opportunities for lightweight, high strength structural design.

### 1. Introduction

The failure strength of sandwich panel structures depends upon many factors including the strength and thickness of the face sheets, the core topology and the parent material. A variety of polymeric foams and honeycombs are used for the cores of stiffness dominated designs. The need for higher strength, impact energy dissipating structures has stimulated the development of stronger metallic foams, see for example [Ashby et al. 2000]. These are mostly produced by the introduction of gas bubbles into the metal [Wadley 2002]. The bubble expansion process leads to random cellular structures, and minimization of surface energy leads to a low nodal connectivity, with typically three to four struts per joint. The resulting mechanical properties are far from optimal due to the fact that the cell walls deform by *local bending* [Deshpande et al. 2001a]. This led to a search for open-cell microstructures which have high nodal connectivities and deform by the *stretching* of constituent cell members, giving a much higher stiffness and strength per unit mass. These cellular solids, known as *lattice materials* — a term we define to

---

*Keywords:* lattice materials, composites, microbuckling, honeycomb, carbon fiber, carbon fibre.

mean any micro-architected cellular solid with straight webs or struts — have a stiffness and strength which scale linearly with relative density  $\bar{\rho}$ ; in contrast, the Young’s modulus and yield strength of metallic foams scale with  $\bar{\rho}^2$  and  $\bar{\rho}^{3/2}$ , respectively. An example of a lattice material is the octet-truss structure with a face-centred cubic microstructure [Deshpande et al. 2001b]. Its joint connectivity is 12, and this spatially periodic material has the feature that the cell members deform by local stretching for all macroscopic loading states. Consequently, the specific mechanical properties (stiffness, strength, toughness and energy absorption) of the Octet-truss far exceed those of open-cell foams. Many variants of this structure have been explored and novel methods for their fabrication and multifunctional properties have been recently reviewed [Wadley 2006].

Examination of the modified Ashby material property chart [Ashby and Bréchet 2003] shown in Figure 1, indicates that aluminium foams and lattices occupy the low density region of material strength- density space. It also reveals a gap between the strength of existing lattice materials and the theoretical attainable material limit. Lattices fabricated from aluminium alloys have begun to extend the range of cellular materials into this gap in the material property space but it is clear that there remains much room for further improvements. Figure 1 illustrates how the combination of optimized lattice topology and parent

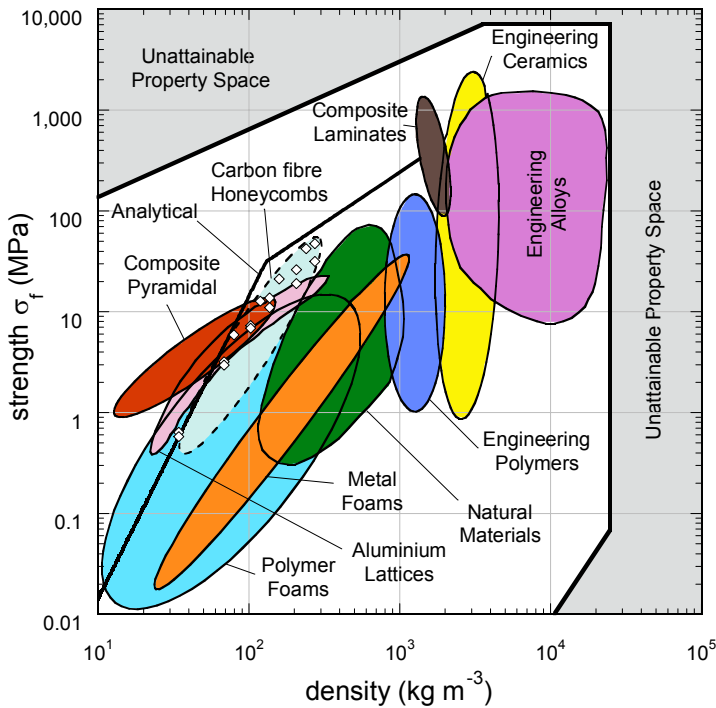


**Figure 1.** An Ashby material strength versus density map for engineering materials [Ashby and Bréchet 2003]. The map contains gaps between existing and unattainable materials. The maximum theoretical strength of composite square honeycombs is shown by the solid line marked *analytical*, which falls into the high specific strength gap at low densities. The measured properties of the composite honeycombs investigated here are also included.

material properties can be combined to expand material property space by creating new engineering materials or cellular structures. For instance, suppose composites containing fibres configured to provide high uniaxial specific strengths were used for the trusses or webs of a lattice structure. If buckling does not occur, the resulting lattice structures have anticipated compressive strengths that fill the gap in the strength versus density space for densities less than about  $100 \text{ kgm}^{-3}$ .

Continuous fibre polymer matrix composites such as carbon-epoxy systems have found extensive use as face-sheets in sandwich construction, particularly in aerospace and sports equipment applications. Typically carbon-epoxy laminate face-sheets are combined with an aluminium hexagonal honeycomb core: the high strength and stiffness per unit mass of carbon-fibre materials boost their ranking in face-sheet materials selection for light-weight structural applications. The use of composites as a core material is a natural progression for increasing the specific strength and stiffness of sandwich structures. The main examples include the Z-fiber and X-Cor<sup>1</sup> truss structures fabricated by angled carbon fibre rods embedded in a polymeric foam; and Nomex-phenolic resin honeycombs which find application in flooring panels for passenger aircraft. There exists little data on such sandwich core materials and that data suggests that the strength per unit mass of these sandwich cores is only marginally better than metallic structures [Marasco et al. 2006].

It is clear that topologically structuring composite materials shows promise for filling gaps in the strength versus density map of all known materials. The aim of the present study is to begin to investigate the expansion of *the strength – density material space* at low densities by using carbon fibre composites to build lattice materials. A related study explored the behaviour of carbon fibre composite lattice structures with an open cell pyramidal truss topology [Finnegan et al. 2007]. The measured peak compressive strengths from that study are included in Figure 1. Clearly the composite pyramidal lattices begin to fill a gap in the known material property space in that they have a strength greater than most known materials at densities less than  $100 \text{ kgm}^{-3}$ . However, the designs of the composite pyramidal cores in [Finnegan et al. 2007] do not achieve the full potential of composite lattice materials primarily due to the inefficient utilization of material in the nodes.

In general three classes of sandwich core architecture have been proposed: (i) prismatic cores, (ii) 3D trusses and (iii) honeycombs. The most suitable choice of sandwich core architecture depends upon the specific application. For example, trusses with their open celled architecture are ideal for multifunctional applications involving heat transfer in addition to load carrying capacity [Evans et al. 1998]. On the other hand, these sandwich cores have a low in-plane stretching strength. Thus, for panels subjected to large bending loads (where in in-plane core stretching is important), stretch resistant cores are superior to the truss cores. Traditionally, hexagonal honeycombs have been extensively employed in sandwich construction; see for example [Gibson and Ashby 1997]. However, hexagonal honeycombs also suffer from a low in-plane stretching strength. Square honeycombs overcome this drawback (at least for loadings along the directions of the cell walls) and thereby have promise for sandwich construction as demonstrated in a number of studies [Côté et al. 2004; Xue and Hutchinson 2004; Fleck and Deshpande 2004]. The out-of-plane compressive and shear deformation of carbon fibre composite square honeycombs is the focus of this study.

---

<sup>1</sup>Z-fiber and X-core are registered trademarks of Aztex Inc., Waltham, MA, USA.

The outline of the paper is as follows. First the composite sheet materials are described along with the route for fabricating the square-honeycombs cores from these materials. Second, the measured compressive and shear responses of the cores are detailed along with the observed failure modes. Analytical and finite element models are then developed for the elastic stiffness and collapse strengths of the composite honeycombs and these are compared with measurements. Finally, the measured strengths of the composite honeycombs are plotted on a map of density versus strength of all known materials in order to gauge the performance of these materials in terms of their strength to weight ratio.

## 2. Materials and manufacture

Square-honeycombs were manufactured from prefabricated composite sheet materials. The methodology follows closely that developed for metallic honeycombs by [Côté et al. 2004].

**2.1. Parent materials.** Two types of carbon fibre composite sheet material with an average sheet thickness  $t = 0.355$  mm were employed in this study. One was a  $\pm 45^\circ$ ,  $2 \times 2$  twill weave (3.7 tows per centimetre and 6000 fibres per tow) panel and the second was a laminate with a 4-ply symmetric balanced  $[0^\circ, 90^\circ]$  lay-up. These two types of materials are referred to as the woven and laminate materials, respectively. In both cases, the composite sheets were made from T300-6k fibres (6–7.5  $\mu\text{m}$  fibre diameter) and a high-heat resistant epoxy matrix (Fiberite 934). The as-fabricated densities of the woven and laminate composites were  $1370 \text{ kgm}^{-3}$  and  $1590 \text{ kgm}^{-3}$ , respectively.

**2.2. Manufacturing route.** Square-honeycombs were manufactured from composite sheets with a thickness  $t = 0.355$  mm using a procedure similar to that developed for metallic honeycombs by [Côté et al. 2004]. The sheets were cropped into rectangles of height  $H$  in the range 26.0 to 124.8 mm and length of 37.8 mm to 256.2 mm. Cross-slots (Figure 2) of width  $\Delta t = 0.40$  mm and spacing  $L$  in the range 5.2 mm to 41.6 mm, were cut using a 2-axis micromill with a mill head capable of cutting slots widths  $\Delta t \geq 200 \mu\text{m}$ . The 45  $\mu\text{m}$  difference between sheet thickness and slot width facilitated assembly while providing a sufficiently tight fit to assure stability. The slotted rectangles were assembled into the square-honeycomb configuration (Figure 2) and adhesively bonded using a low viscosity epoxy resin (Opti-tec 5001<sup>2</sup>). The assembly was then cured at  $65^\circ \text{C}$  for 1 hour. Mild steel face sheets of thickness 3 mm were finally bonded to the top and bottom faces of the honeycomb using a nylon backed film epoxy (Redux 319<sup>3</sup> with an areal density  $400 \text{ gm}^{-2}$ ) and the entire assembly again oven cured at  $175^\circ \text{C}$  for 1 hour.

The relative density  $\bar{\rho}$  of the square-honeycomb is to first order given by

$$\bar{\rho} = \frac{2t}{L}, \quad (1)$$

and honeycomb specimens of different densities were manufactured by varying the cell size  $L$  while keeping the wall thickness always fixed at the sheet thickness  $t = 0.355$  mm. An example of a manufactured square-honeycomb (without the steel face-sheets) made from the woven material with  $\bar{\rho} = 0.05$ , comprising  $6 \times 6$  cells and a cell aspect ratio  $H/L = 3$  is shown in Figure 3.

<sup>2</sup>Intertronics, 17 Station Field Industrial Estate, Banbury Road, Kidlington, Oxfordshire, OX5 1JD, UK.

<sup>3</sup>Hexcel Composites, Duxford UK.

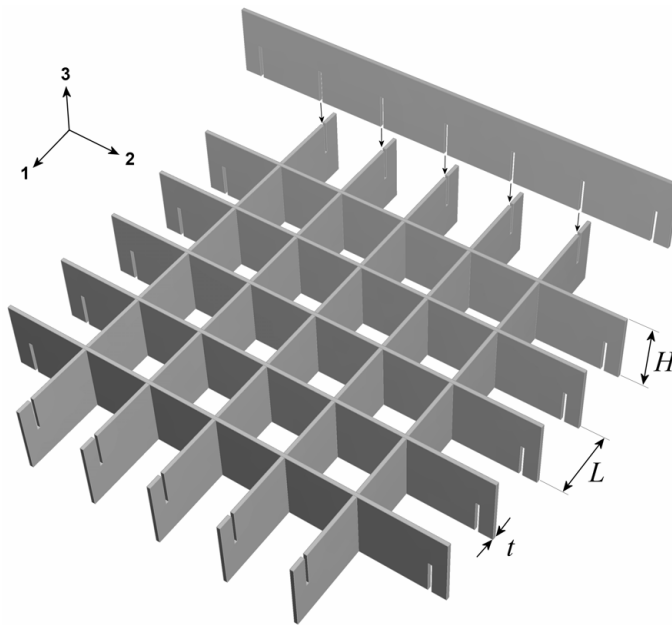


**Figure 2.** Sketch of the square-honeycomb manufacturing technique. The coordinate system associated with the honeycomb and the notation used to indicate the dimensions of the honeycomb are also shown.

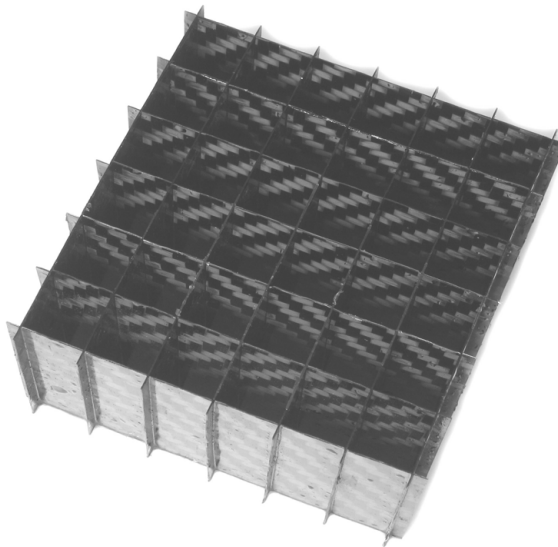


**Figure 3.** Photograph of the  $\bar{\rho} = 0.05$  square-honeycomb made from the 0–90° woven material and comprising  $6 \times 6$  cells with a cell aspect ratio  $H/L = 3$ .

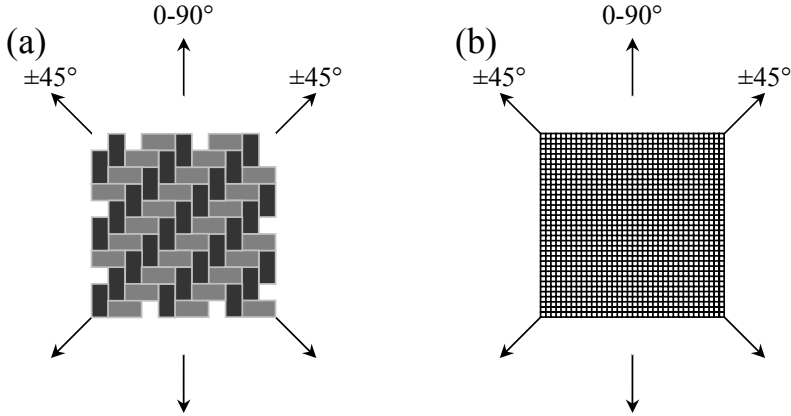


**Figure 4.** Sketch illustrating the 0–90° and ±45° orientations in which compression and tensile tests were conducted on the parent (a) woven and (b) laminate materials.

### 3. Mechanical measurements

**3.1. The parent materials.** Tensile and compression tests were conducted on the woven and laminate materials in two directions, labelled 0–90° and ±45° in Figure 4. The angles denote the directions along which the fibres lie with respect to the tensile or compression axes.

Rectangular tensile specimens of dimension 20 mm × 140 mm were cut from the composite sheets and aluminium tabs of dimension 20 mm × 40 mm were bonded to the ends of the specimens to facilitate gripping. Tensile tests were conducted in a screw driven test machine at an applied nominal strain rate  $10^{-3} \text{ s}^{-1}$  with the applied load measured via the load cell of the test machine and the strain inferred from displacements measured using a laser interferometer. The measured tensile responses in the 0–90° and ±45° directions are plotted in Figure 5. In the 0–90° direction the composites exhibit an approximately

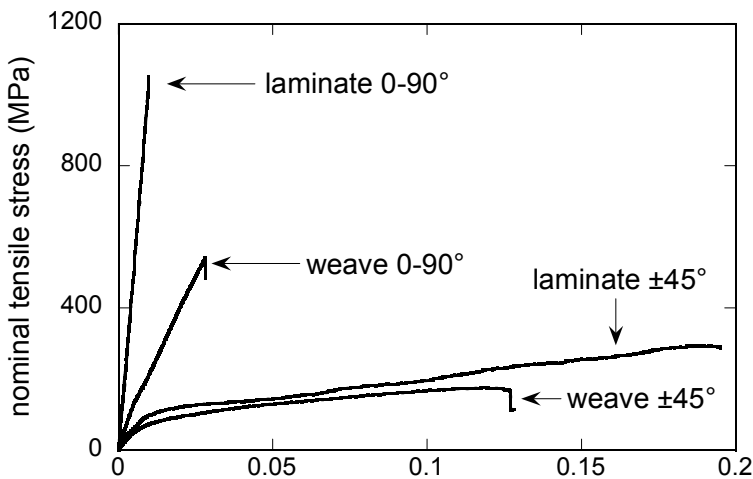


**Figure 5.** The measured uniaxial tensile responses of the woven and laminate composite materials in the 0–90° and ±45° orientations.

linear response prior to failure. The peak strengths of the woven and laminate materials were 558 MPa and 1.05 GPa, respectively and their corresponding tensile ductilities 2.98% and 0.97%. Both materials exhibited significantly greater ductility when loaded in the  $\pm 45^\circ$  direction with failure strains of 12% and 19% for the woven and laminate materials, respectively. However, this was accompanied by significantly reduced peak strengths of 161 MPa (woven) and 294 MPa (laminate). These differences arise from the fibre orientation: in the  $\pm 45^\circ$  direction, matrix deformation dominates the response, while in the  $0-90^\circ$  direction the is load primarily sustained by the fibres.

The small sheet thickness of the composites employed in this study meant that it was difficult to conduct standard Celanese type compression tests on these materials while avoiding macrobuckling of the specimens. Thus, the specimens were tested using a sandwich column configuration as sketched in Figure 6a. The sandwich specimens were constructed by epoxy bonding the composite sheets to an aluminium hexagonal honeycomb core of relative density 6%, cell size 6.35 mm and wall thickness 0.381 mm. These specimens were then cut into a dog-bone configuration with dimensions as sketched in Figure 6a. This configuration had a high bending stiffness to obviate the possibility of macrobuckling. Moreover, the in-plane compression of the hexagonal honeycomb core had a negligible contribution to the measured loads. Strain gauge rosettes were bonded to both face-sheets of the sandwich column to measure the compressive strains in the face-sheets (and their Poisson expansion) and the stress in each of the composite sheets was deduced from the load cell of the test machine. The compression tests were conducted at an applied nominal strain rate  $10^{-3} \text{ s}^{-1}$ . The strains in both face-sheets were observed to be within 10% of each other. This confirmed that the sandwich columns underwent negligible bending and thus the measurements are representative of the compressive responses of the composite sheets. The compressive stress versus strain responses of the woven and laminate sheet materials in the  $0-90^\circ$  and

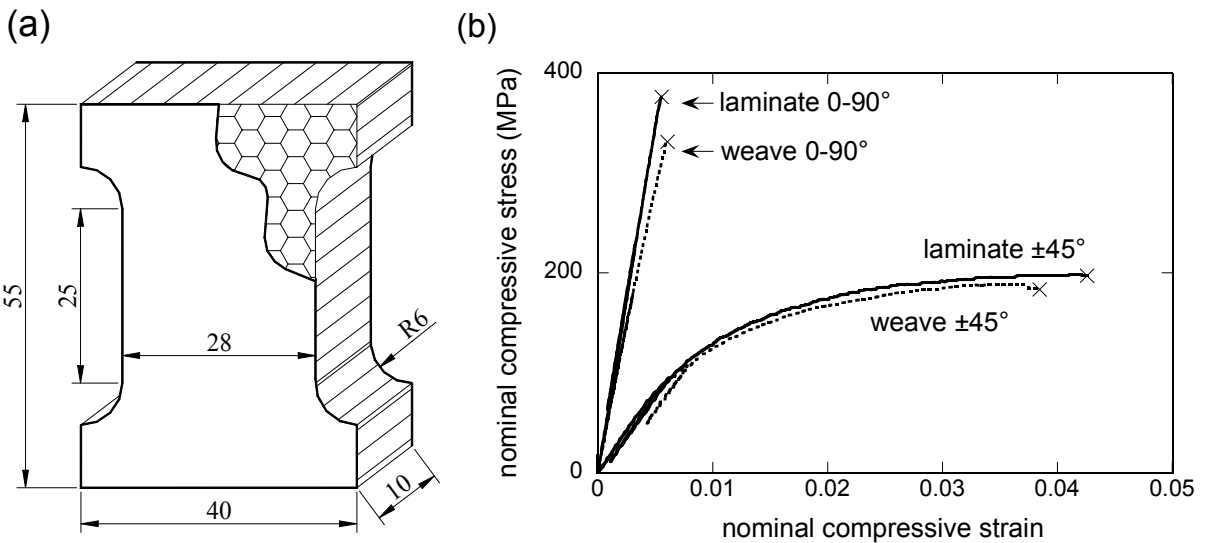


**Figure 6.** (a) Sketch of the sandwich column configuration used to conduct compression tests on the composite sheet materials. All dimensions are in mm. (b) The measured uniaxial compressive responses of the woven and laminate composite materials in the  $0-90^\circ$  and  $\pm 45^\circ$  orientations.

$\pm 45^\circ$  directions are plotted in Figure 6b. Similar to the tensile responses, the composite sheets have a high strength but low failure strain in the 0–90° direction and vice-versa in the  $\pm 45^\circ$  direction. Interestingly, both the woven and laminate materials have approximately the same compressive strength in the 0–90° direction suggesting that fibre waviness even in the laminates significantly reduces its peak compressive strength. We note that in the 0–90° direction, the composite sheets have a lower compressive strength compared to the tensile strength due to the fact that the tensile strength is governed by the failure strength of the fibres while the compressive strength of the materials is governed by fibre waviness which causes microbuckling failure of the composite materials.

**3.2. Compressive response of the honeycombs.** Compressive tests were conducted on the composite square honeycombs to investigate the effects of (i) relative density  $\bar{\rho}$ , (ii) parent material type and orientation, (iii) cell geometry as characterized by the aspect ratio  $H/L$  and (iv) number of cells in the compressive test specimen. The compression tests were conducted in a screw driven test machine at a nominal applied strain rate  $10^{-3} \text{ s}^{-1}$ . The compressive stress was inferred from the load cell output of the test machine while the average compressive strain was deduced from laser interferometer measurements of the relative approach of the two steel face sheets of the test specimens. A few loading-unloading cycles were conducted during each test in order to infer the compressive Young’s modulus of the honeycombs. At least one repeat test was conducted on each of the specimens in order to confirm the repeatability of the results presented subsequently.

**3.2.1. Effect of specimen geometry.** The majority of the tests were conducted on square-honeycomb specimens manufactured from the woven composite material oriented such that one set of fibres was aligned with the compression direction; such square-honeycombs are referred to as the 0–90° woven honeycombs and the effect of specimen geometry is investigated using these types of honeycombs. The

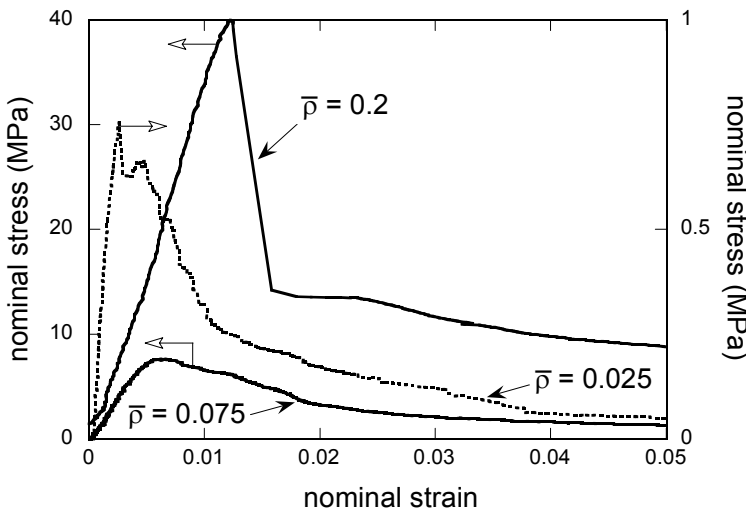


**Figure 7.** Measured compressive stress versus strain response of the honeycombs made from the 0–90° woven composite material for selected values of the specimen relative densities  $\bar{\rho}$ . All measurements are reported on specimens with  $6 \times 6$  cells and  $H/L = 3$ .

$\bar{\rho}$	aspect ratio ( $H/L$ )		
	1	3	5
0.025	6×6	4×4, 6×6	–
0.05	6×6	4×4, 6×6, 12×12	–
0.075	6×6	4×4, 6×6, 12×12	–
0.1	6×6	4×4, 6×6, 12×12	6×6
0.15	–	4×4, 6×6, 12×12	6×6
0.2	–	4×4, 6×6, 12×12	6×6

**Table 1.** List of the types of square-honeycomb specimens made from the woven composite material (0–90° orientation) that were manufactured and tested in compression in this study. The number of cells in each of the specimen types is indicated in the table.

range of 0–90° woven honeycomb specimens investigated here are summarized in Table 1 (the table lists the number of cells in the specimen for each value of  $H/L$  and  $\bar{\rho}$  investigated). The range of samples tested was limited by the use of sheets with a thickness  $t = 0.355$  mm to make all specimens. This implies that (i) low density specimens with a high value of  $H/L$  are extremely large and thus impractical to test in a laboratory setting (e.g.  $\bar{\rho} = 0.025$  and  $H/L = 5$ ) and (ii) high density specimens with a low value of  $H/L$  are too small to manufacture with any degree of accuracy (e.g.  $\bar{\rho} = 0.2$  and  $H/L = 1$ ). Even so, a sufficiently wide range of specimen geometries were tested to make the necessary inferences about the effects of specimen geometry. The reference test geometry comprised  $6 \times 6$  cells with an aspect ratio  $H/L = 3$ . Unless otherwise specified, this reference geometry was employed in all tests.

The measured compressive stress versus strain response of the 0–90° woven honeycombs is plotted in Figure 7 for selected values of the relative density  $\bar{\rho}$ . The response is reasonably linear up to the peak stress. The subsequent softening beyond the peak stress is rather dramatic for the  $\bar{\rho} = 0.2$  case suggesting a microbuckling failure of the composite sheets. By contrast, the stress falls more gradually for the lower density honeycombs suggesting a failure by elastic buckling of the honeycomb webs.

Evidence for buckling is seen in the montage of photographs of the  $\bar{\rho} = 0.05$  specimen at selected levels of applied compressive strain (Figure 8a). The associated compressive stress versus strain curve is plotted in Figure 8b. The deformation of the cell walls is essentially uniform for strains less than about 0.3%. Distinct wrinkling of the cell walls is observed at larger strains due to the onset of buckling. Now consider the  $\bar{\rho} = 0.2$  honeycomb. As discussed above we anticipate that the high density honeycombs ( $\bar{\rho} = 0.2$ ) undergo microbuckling failure. However, this mode of failure is not evident in the image shown in Figure 9a, as the cell walls towards the edge of the specimen are unconstrained and thus undergo a macrobuckling collapse mode. However, we expect the constrained cell walls in the interior of the

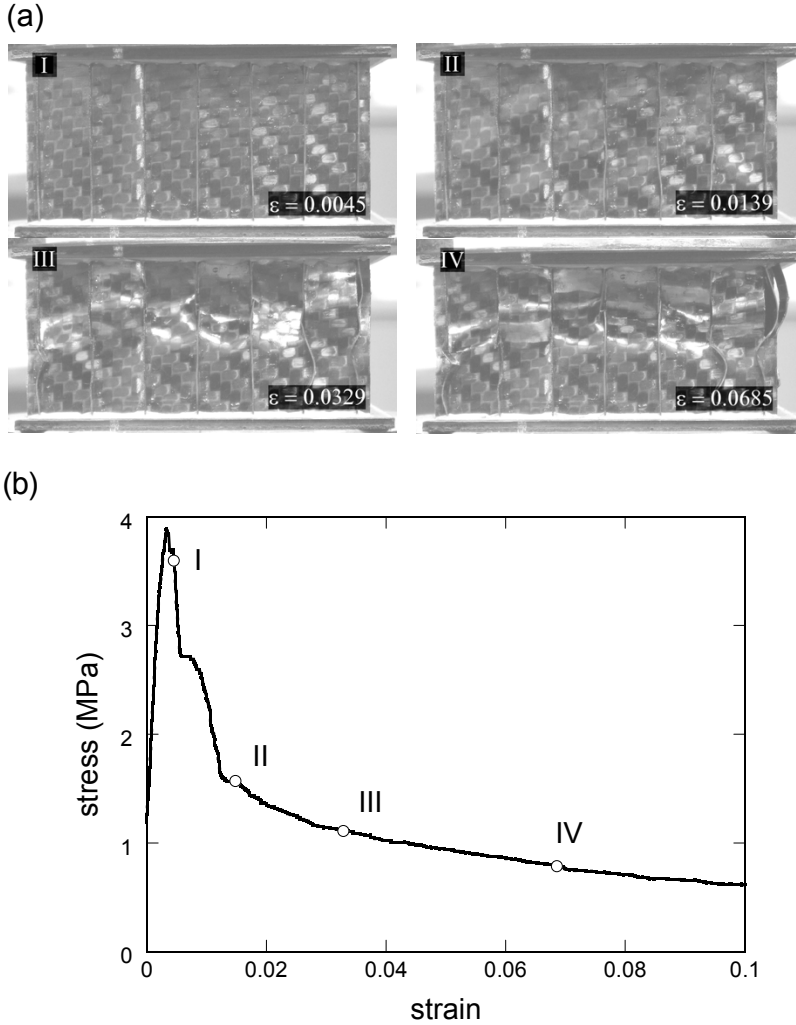


**Figure 8.** (a) Photographs at selected values of the compressive strain  $\epsilon$  showing the compressive deformation mode of the  $\bar{\rho} = 0.05$  honeycomb made from the 0–90° woven composite material. (b) Associated measured compressive stress versus strain response.

specimen to fail by microbuckling. In order to test this hypothesis we used X-ray tomography to observe the failure mechanism in the  $\bar{\rho} = 0.2$  ( $H/L = 3$ ) specimen comprising  $4 \times 4$  cells. The specimen was compressed using the fixture sketched in Figure 10. The specimen was first compressed to the required strain in the screw-driven test machine and the bolts on the fixture tightened so that the specimen did not unload upon removal from the test machine. The specimen was then scanned using a X-ray tomography system. This procedure was repeated for four values of applied strain as marked on the measured stress versus strain response included in Figure 9b. The X-ray images along the two sections marked in Figure 9a are shown in Figure 11 at the four levels of applied strain indicated in Figure 9b. The contrast between the middle and edge of the specimen is evident in Figure 11: (i) the cell walls bend near the edge of the specimen, prior to the peak stress, while they remain straight in the middle of the specimen; (ii) just

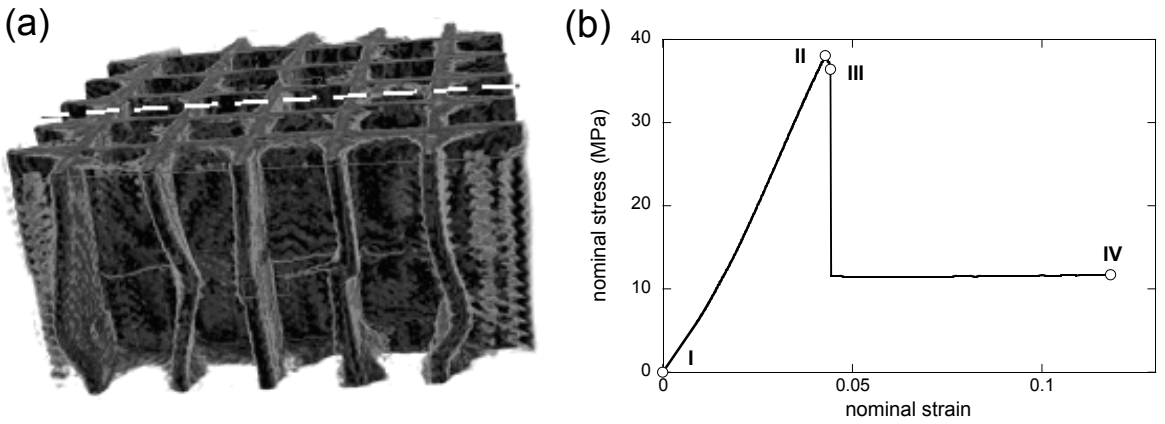


**Figure 9.** Compressive deformation modes of the  $\bar{\rho} = 0.2$  honeycomb made from the 0–90° woven composite material. The specimen comprised  $4 \times 4$  cells. (a) Photograph of the specimen deformed to a strain  $\varepsilon = 0.12$ . The sections along which the X-ray images are taken are also marked. (b) The measured compressive stress versus strain response with the strains at which X-ray images were taken labelled on the plot.

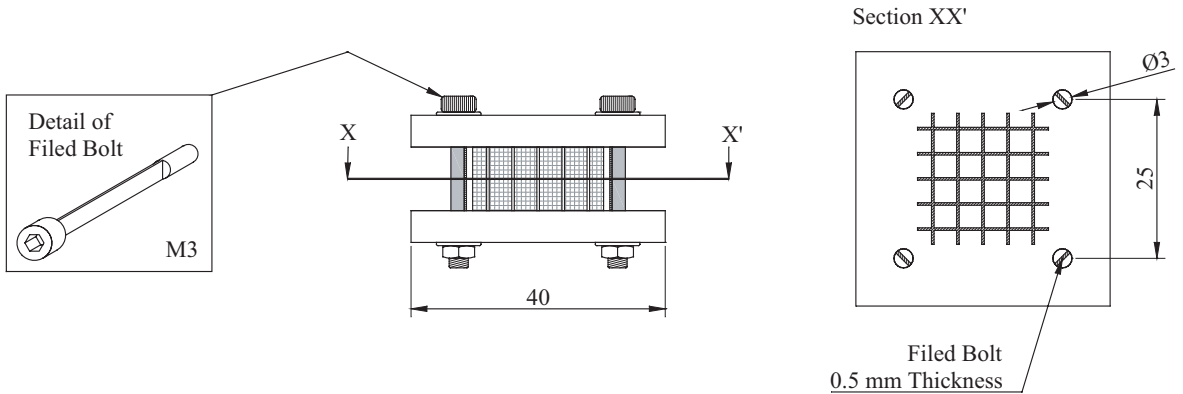


**Figure 10.** Sketch of the fixture used to compress the specimen used and then scan in X-ray tomography system. The fixture prevents unloading of the specimen when it is removed from the test machine.

beyond the peak stress a small kink is seen to develop in the cell walls in the middle of the specimen that is reminiscent of a microbuckle failure.

The measured unloading modulus  $E$  and peak stresses  $\sigma_p$  of the honeycomb specimens with  $6 \times 6$  cells are plotted in Figure 12 as a function of the relative density  $\bar{\rho}$ , for three values of  $H/L$ . Note that for  $H/L = 1$  and  $H/L = 5$  data does not exist for some values of  $\bar{\rho}$ , as detailed in Table 1. Nevertheless the trends are clear: both  $E$  and  $\sigma_p$  increase approximately linearly with increasing  $\bar{\rho}$  while the cell aspect ratio  $H/L$  has a negligible effect for the range of aspect ratios considered here.

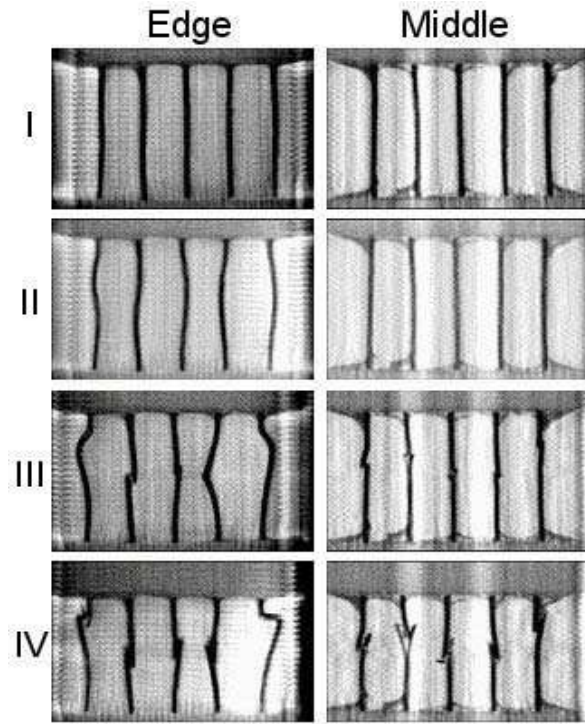


**Figure 11.** X-ray images of the honeycomb specimen along the two sections marked in Figure 9a and strain values indicated in Figure 9b.

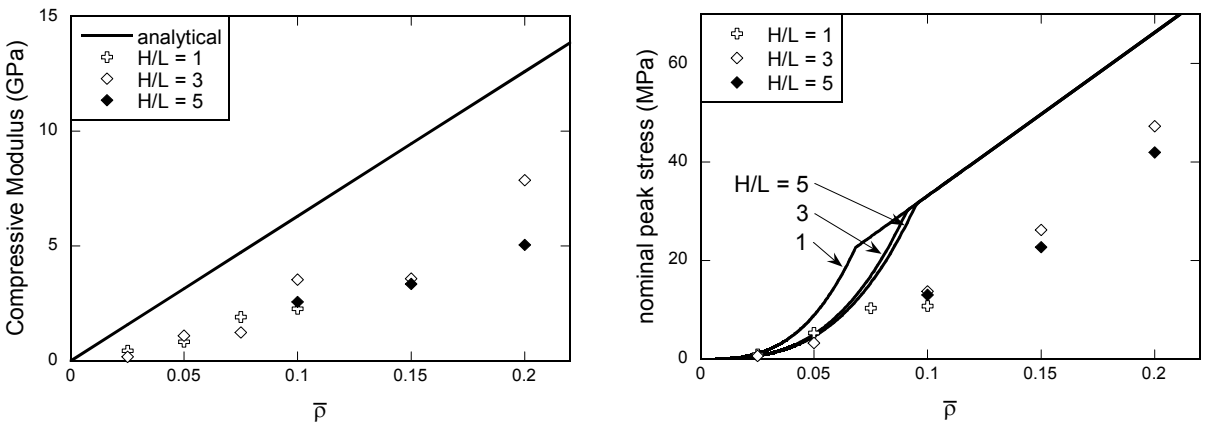


**Figure 12.** The measured Young’s modulus  $E$  (left) and peak strength  $\sigma_p$  (right) of the honeycombs made from the 0–90° woven composite material as a function of the relative density  $\bar{\rho}$ . Measurements are shown for specimens comprising  $6 \times 6$  cells and selected values of the aspect ratio  $H/L$ . The predictions of the analytical models are also included as solid lines.

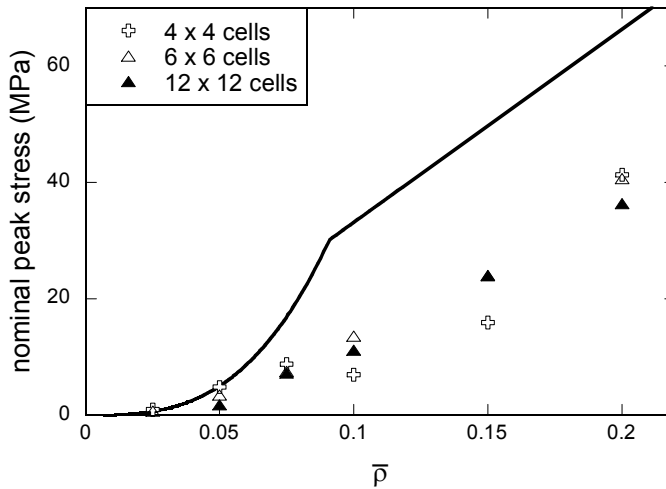


**Figure 13.** Measured peak strength  $\sigma_p$  of the honeycombs made from the 0–90° woven composite material as a function of the relative density  $\bar{\rho}$ . Measurements are shown for specimens with a cell aspect ratio  $H/L = 3$  and for specimens with  $4 \times 4$ ,  $6 \times 6$  and  $12 \times 12$  cells. Predictions of the analytical model are also included.

The X-ray tomographs in Figure 11 show that the deformation modes of the cell walls in the middle of the specimen and towards the specimen edge differ substantially. This suggests that the measured compressive response of the honeycombs might be sensitive to the number of cells in the specimens. In addition to the reference value of  $6 \times 6$  cells, tests were conducted on honeycomb specimens comprising  $4 \times 4$  and  $12 \times 12$  cells, all with an aspect ratio  $H/L = 3$ . The measured peak stresses  $\sigma_p$  from these tests are plotted in Figure 13 as a function of  $\bar{\rho}$ . The measurements from specimens with  $6 \times 6$  and  $12 \times 12$  cells are almost identical confirming that the reference specimen employed in this study provides data that is reasonably independent of the number of cells in the specimens. However, the measured peak strengths from the specimens with  $4 \times 4$  cells were slightly lower than those of the  $6 \times 6$  and  $12 \times 12$  cell specimens suggesting that edge effects play a more dominant role in the deformation of the  $4 \times 4$  (and smaller) cell specimens.

**3.2.2. Effect of material type and orientation.** The measured compressive stress  $\sigma$  versus strain  $\varepsilon$  response of the composite square honeycombs made from the laminate material with fibres at 0–90° with respect to the compression axis and the woven composite material oriented in the  $\pm 45^\circ$  direction (such that the fibres were at  $\pm 45^\circ$  with respect to the compression direction) are plotted in Figure 14 for selected values of  $\bar{\rho}$ . These measurements were conducted on the reference specimen geometry comprising  $6 \times 6$  cells with  $H/L = 3$ . Consistent with the measured compressive responses of the materials (Figure 7), the honeycombs made from  $\pm 45^\circ$  weave have a lower strength compared to the 0–90° laminate honeycombs. On the other hand, the  $\pm 45^\circ$  woven honeycombs display a more gradual softening beyond the peak stress compared to the 0–90° laminate honeycombs. This is because the compressive response of the 0–90° laminate is dominated by the compression of the fibres, while that of the  $\pm 45^\circ$  weave is dominated by matrix deformation.

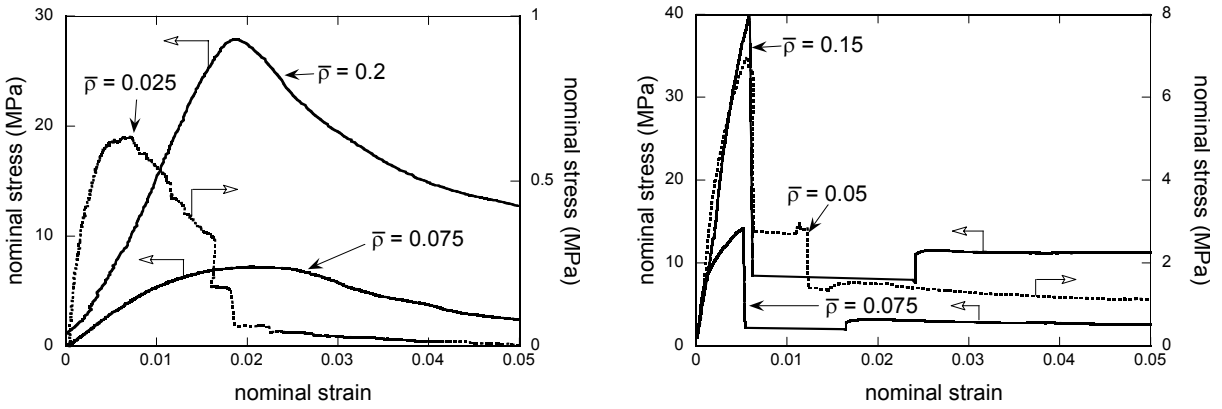


**Figure 14.** The measured compressive stress versus compressive strain responses of the honeycombs made from the  $\pm 45^\circ$  woven material (left) and the  $0-90^\circ$  laminate material (right). Results are shown for selected values of  $\bar{\rho}$  for specimens comprising  $6 \times 6$  cells and a cell aspect ratio  $H/L = 3$ .

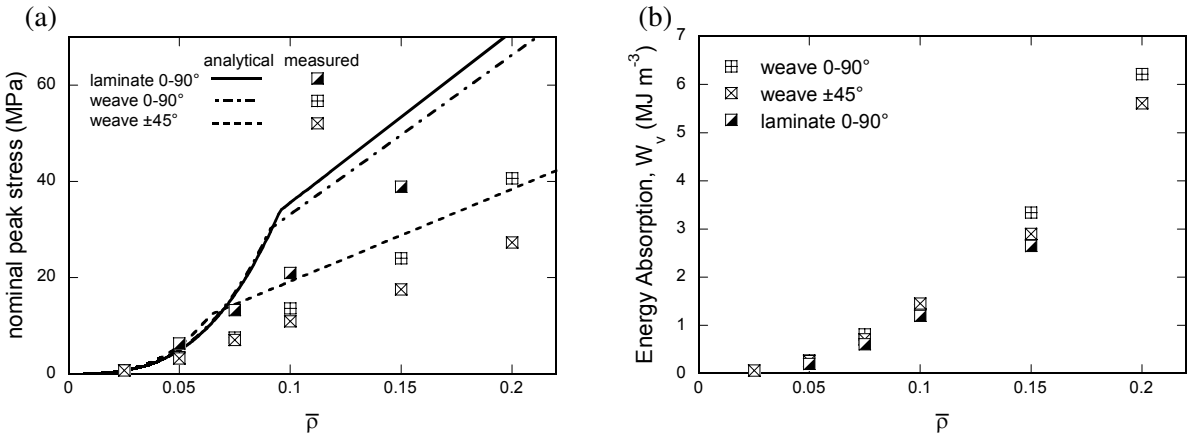


**Figure 15.** A comparison of the measured (a) peak compressive strengths  $\sigma_p$  and (b) energy absorption capacities per unit volume  $W_v$  of the honeycombs made from the  $\pm 45^\circ$  woven,  $0-90^\circ$  woven and  $0-90^\circ$  laminate materials as a function of  $\bar{\rho}$ . The measurements are for specimens comprising  $6 \times 6$  cells and a cell aspect ratio  $H/L = 3$ , compressed to a strain of 40%.

The measured peak compressive strengths of honeycombs (reference geometry) made from the  $0-90^\circ$  weave,  $0-90^\circ$  laminate and  $\pm 45^\circ$  weave are compared in Figure 15a for relative densities in the range  $0.025 \leq \bar{\rho} \leq 0.2$ . Consistent with our expectations from the measured compressive responses of these materials (Figure 7) we observe that for a given value of  $\bar{\rho}$  the  $0-90^\circ$  laminate has the highest value of  $\sigma_p$  followed by the  $0-90^\circ$  weave with the honeycomb made from the  $\pm 45^\circ$  having the lowest value of peak strength. However, recall that honeycombs made from materials with the  $0-90^\circ$  fibre orientation

typically undergo a catastrophic collapse beyond the peak stress and loose all energy absorption capacity, while the honeycombs made from the  $\pm 45^\circ$  woven materials have a more benign response beyond the peak stress. These differences are expected to alter the rankings of the materials in terms of their energy absorption capacity per unit volume  $W_v$  defined as

$$W_v = \int_0^{\bar{\epsilon}} \sigma d\epsilon. \tag{2}$$

$W_v$  is plotted in Figure 15b with the choice of strain  $\bar{\epsilon} = 0.4$  as a function of  $\bar{\rho}$  for the three configurations considered in Figure 15a. The results indicate that honeycombs made from the  $0-90^\circ$  weave,  $0-90^\circ$  laminate and  $\pm 45^\circ$  weave all have approximately the same energy absorption capacity per unit volume over the range of  $\bar{\rho}$  investigated here. This is rationalised by noting that the lower peak strength of the  $\pm 45^\circ$  woven honeycomb is compensated by its higher energy absorption beyond its peak stress compared to the honeycombs with a  $0-90^\circ$  fibre orientation.

**3.3. Shear response of the honeycombs.** A more limited study was conducted to investigate the out-of-plane shear stress  $\tau_{31}$  versus shear strain  $\gamma_{31}$  response of the composite honeycombs made from the woven material with a cell aspect ratio  $H/L = 1$ . The shear tests were conducted using a single-lap shear set-up (Figure 16) in accordance with the ASTM standard C273-00 [ASTM 2000] for shear tests on sandwich cores. The standard demands a specimen aspect ratio  $\ell/H \geq 12$ , where  $\ell$  is the length of the specimen as shown in Figure 16. The shear specimens investigated here comprised 14 and 4 cells along the length and width, respectively. Thus, in line with the requirements of the ASTM standard, the shear specimens employed here have an aspect ratio  $\ell/H = 14$ . The shear tests were performed on a screw driven test machine at an applied macroscopic nominal shear strain-rate of  $10^{-3} \text{ s}^{-1}$ . The load was measured by the load cell of the test machine and was used to define the nominal shear stress, while a clip gauge mounted on the single-lap shear test fixture was employed to measure the relative displacement between the two faces of the square honeycomb specimens and thereby give the applied shear strain. Load/unload cycles were also conducted during these tests in order to extract the unloading shear moduli of the specimens.

The measured shear responses of the honeycombs made from the  $0-90^\circ$  and  $\pm 45^\circ$  woven materials are plotted in Figure 17. Again, in the  $0-90^\circ$  orientation one set of fibres are aligned with the plane of shear while in the  $\pm 45^\circ$  orientation the fibres are at  $\pm 45^\circ$  with respect to this plane. Three relative densities  $\bar{\rho} = 0.025, 0.05$  and  $0.1$ , were investigated. The  $0-90^\circ$  specimens display a ductile response

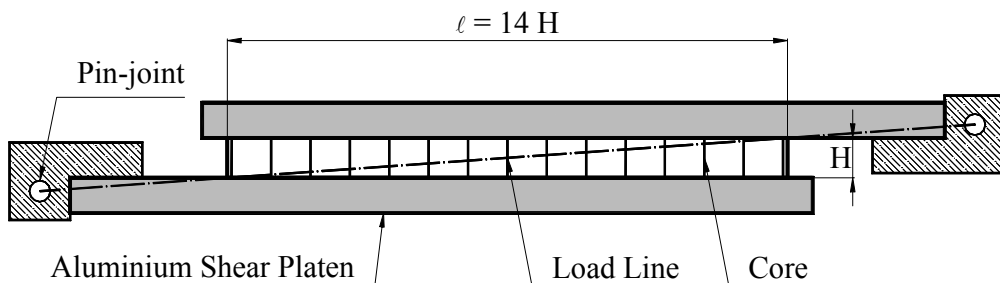


**Figure 16.** Sketch of the single-lap shear set-up with the critical dimensions labelled.

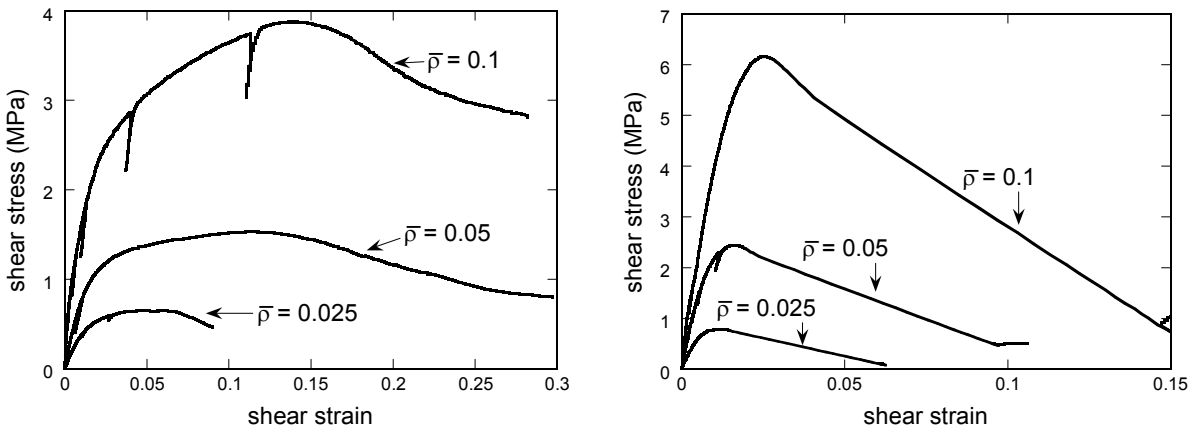


**Figure 17.** The measured shear stress versus shear strain response of the honeycombs made from the 0–90° (left) and ±45° (right) woven materials at selected values of  $\bar{\rho}$ . All the shear specimens comprised  $14 \times 4$  cells with a cell aspect ratio  $H/L = 1$ .

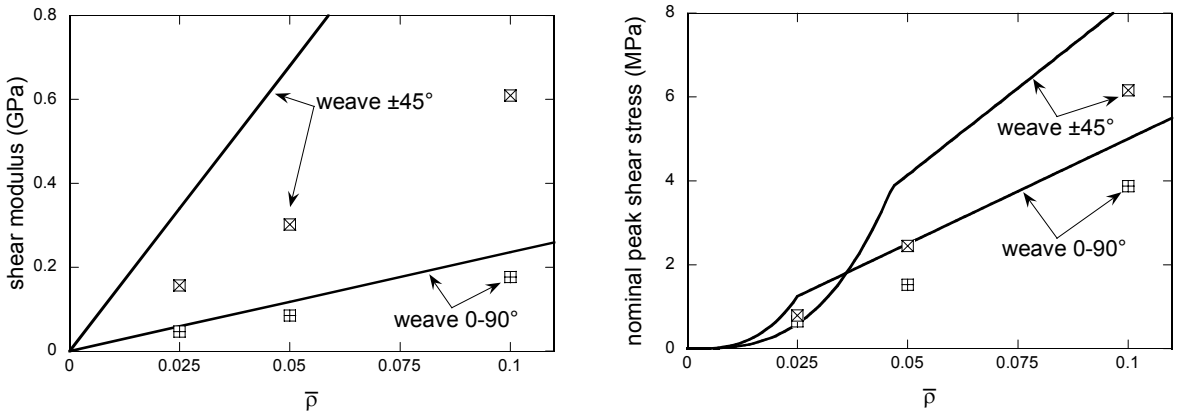


**Figure 18.** The measured shear modulus (left) and peak shear strength  $\tau_p$  (right) of the honeycombs made from the 0–90° and ±45° woven materials. The predictions of the analytical model are also included as solid lines.

reminiscent of the tensile and compressive response of the ±45° woven material (Figures 5 and 6b). By contrast, the ±45° specimens display a stiff linear response up to their peak strength similar to the tensile and compressive responses of the woven material in the 0–90° orientation; post-peak a strongly softening response is observed. Moreover, the ±45° specimens have a significantly higher peak shear strengths compared to equal density 0–90° honeycomb specimens. These results clearly indicate that the shear response of the 0–90° specimens is dominated by the deformation of the matrix of the woven composites while the fibres govern the shearing of ±45° specimens. The measured shear moduli and peak shear strengths are plotted in Figure 18 as a function of  $\bar{\rho}$ . The modulus and strength of both the 0–90° and ±45° specimens increases with increasing  $\bar{\rho}$  with the ±45° honeycombs being stiffer and stronger than the 0–90° honeycombs.

#### 4. Analytical models for the compressive and shear response

Approximate expressions can be derived for the elastic properties and collapse strengths of the composite honeycombs subject to the compressive and shear loadings described above. The properties for the composite sheet are denoted by a subscripted  $s$ .

**4.1. Compression response.** Under compressive loading, all cell walls of the honeycomb are equally loaded. Thus, when the honeycomb is subjected to an out-of-plane compressive stress,  $\sigma$ , each cell wall is subjected to a line load  $P$  per unit length

$$P = \sigma \frac{L}{2}, \tag{3}$$

where  $L$  is the cell width (Figure 2). The Young’s modulus  $E$  of the square honeycombs then follows as

$$\frac{E}{E_{3s}} = \bar{\rho}, \tag{4}$$

where  $E_{3s}$  is the Young’s modulus of the composite sheet material in the  $x_3$ -direction.

The peak compressive strength of the honeycombs is governed by a competition between (i) elastic buckling and (ii) plastic microbuckling of the cell walls. We consider each of these modes in turn.

A recent experimental study [Côté et al. 2004] on the compressive collapse of square honeycombs made from type 304 stainless steel suggests that the elastic buckling mode resembles torsional-axial buckling of a square tube, as shown in Figure 19 representing a view of a section through the plane normal to  $x_3$ . We expect this mode to exist for the composite honeycombs investigated here. This buckling mode is modelled by the buckling of a single plate with fully clamped top and bottom edges and simply supported sides. [Ericksen and March 1958] have analysed this reduced problem for a plate

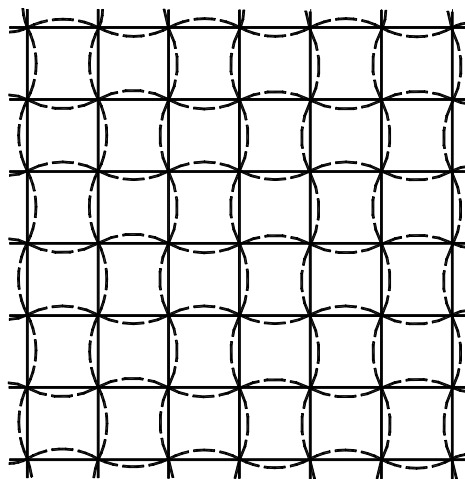


**Figure 19.** Sketch of the torsional buckling mode of the square honeycombs used in deriving the analytical models for the elastic buckling of the honeycombs. The undeformed honeycomb is shown by the solid lines and the buckle shape sketched with dashed lines.

made from orthotropic faces, and use their analytical results directly. The bifurcation line load reads

$$P_{\text{buck}} = \frac{K\pi^2 D}{L^2}, \tag{5}$$

where  $K$  is a buckling coefficient as prescribed by [Eriksen and March 1958] and  $D$  is the bending stiffness of the composite cell wall. In our problem, we assume the composite to be an orthotropic material and the appropriate bending stiffness  $D$  is given as

$$D = \frac{\sqrt{E_{1s}E_{3s}}}{1 - \nu_{13s}\nu_{31s}} \frac{t^3}{12},$$

where  $E_{is}$  and  $\nu_{ijs}$  are the Young’s modulus and Poisson’s ratios of the orthotropic faces along the  $x_i = (x_1, x_3)$  directions as defined in Figure 2. For both the  $0\text{--}90^\circ$  and  $\pm 45^\circ$  materials the Young’s moduli are equal along directions  $x_1$  and  $x_3$ .

The formula for the buckling coefficient  $K$  is explicit and for the assumed buckling mode sketched in Figure 19 is given by

$$K = \left( \frac{3H^2}{4L^2} \sqrt{\frac{E_{1s}}{E_{3s}}} + 2\beta + \frac{41L^2}{5H^2} \sqrt{\frac{E_{3s}}{E_{1s}}} \right), \tag{6}$$

where  $\beta$  is given in terms of the shear modulus  $G_{13s}$  as

$$\beta = \frac{1 - \nu_{13s}\nu_{31s}}{\sqrt{E_{1s}E_{3s}}} \left( \frac{E_{1s}\nu_{31s}}{1 - \nu_{13s}\nu_{31s}} + 2G_{13s} \right). \tag{7}$$

The elastic buckling stress of the honeycomb then follows from Equation (3) as

$$\sigma_{\text{buck}} = \frac{2P_{\text{buck}}}{L} = \frac{P_{\text{buck}}\bar{\rho}}{t}. \tag{8}$$

The cell walls of the square honeycombs can also fail by plastic microbuckling. With the plastic microbuckling stress of the cell wall material in the  $x_3$ -direction given by  $\sigma_c$ , collapse stress of the honeycomb is given by

$$\sigma_{mb} = \bar{\rho}\sigma_c. \tag{9}$$

The operative collapse mode of the honeycombs is the one associated with the lowest load, and thus the peak stress  $\sigma_p$  of the honeycombs is

$$\sigma_p = \min(\sigma_{mb}, \sigma_{\text{buck}}). \tag{10}$$

**4.2. Shear response.** Under a shear stress  $\tau_{31}$ , the cell walls of the square honeycomb in the plane normal to  $x_2$  undergo shear straining while the walls in the plane normal to  $x_1$  deform by bending and carry a negligible fraction of the load. Thus neglecting the contribution of the cell walls in the plane normal to  $x_1$ , the overall shear modulus of the square honeycombs is given as

$$\frac{G}{G_{31s}} = \frac{\bar{\rho}}{2}, \tag{11}$$

in terms of the shear modulus  $G_{31s}$  of the composite sheet material. The peak shear strength of the honeycombs is again governed either by the elastic buckling of the cell walls or by the shear strength  $\tau_{31s}$  of the composite sheet material when subjected to a shear stress  $\tau_{31}$ . We consider each of these mechanisms in turn.

Consider the elastic buckling of the cell walls that lie along the  $x_1$ -direction direction. The principal bending rigidities of this cell wall are given as

$$D_1 = \frac{E_{1s}t^3}{12(1 - \nu_{13s}\nu_{31s})}, \quad D_3 = \frac{E_{3s}t^3}{12(1 - \nu_{31s}\nu_{13s})}, \quad D_{31} = \frac{G_{31s}t^3}{12}. \quad (12)$$

The elastic shear buckling stress of a plate clamped along the edges  $x_3 = 0$  and  $x_3 = H$  and simply supported along the other two edges is given in terms of the above rigidities as [Seydel 1930]

$$\tau_b = K_s \frac{\pi^2}{tL^2} \sqrt[4]{D_1 D_3^3}. \quad (13)$$

In this case the factor  $K_s$  is only a function of the nondimensional group

$$\eta \equiv \frac{D_{31}}{\sqrt{D_1 D_3}}, \quad (14)$$

and lies in the range  $7 \leq K_s \leq 14$  for  $\eta$  in the range 0 to 2.0 as specified in [Krivetsky 1959]. The elastic buckling strength of the honeycomb then follows as

$$\tau_{\text{buck}} = \tau_b \frac{\bar{\rho}}{2}. \quad (15)$$

When the peak stress of the honeycomb is governed by the shear failure of the composite material, the strength  $\tau_s$  of the honeycombs is given in terms of the strength  $\tau_{31s}$  of the cell wall material as

$$\tau_s = \tau_{31s} \frac{\bar{\rho}}{2}. \quad (16)$$

Combining, Equations (15) and (16), the peak shear strength of the honeycombs is

$$\tau_p = \min(\tau_s, \tau_{\text{buck}}). \quad (17)$$

Note that this analysis remains unchanged for shear loading  $\tau_{32}$ .

**4.3. Extraction of material properties.** The compressive tests on the sandwich specimen described in Section 3.1 were used to extract the material properties required to use in the models discussed above. The moduli  $E_{1s} = E_{3s}$ , and peak compressive strength  $\sigma_c$  for the woven and laminate materials follow directly from the measurements plotted in Figure 7 for the materials in the 0–90° and ±45° orientations. The Poisson’s ratios  $\nu_{13s} = \nu_{31s}$  were also measured in these tests using strain gauge rosettes (see Section 3.1). These measured material properties for the woven and laminate materials are listed in Table 2.

The required shear elastic properties of the composite sheets were estimated from compression tests conducted by rotating the composite sheet material through 45° as described subsequently. In order to determine the shear modulus  $G_{31s}$  of the woven material in the 0–90° orientation, consider the compression test on the ±45° woven material plotted in Figure 7. Write the applied compressive stress as  $\sigma_x$ , and the corresponding axial strain and transverse strains as  $\varepsilon_x$  and  $\varepsilon_y$ , respectively. Then, the required shear stress  $\tau$  versus shear strain  $\gamma$  relation is obtained via the connections  $\tau = \sigma_x/2$  and  $\gamma = \varepsilon_x - \varepsilon_y$ . The shear modulus  $G_{31s}$  follows immediately as the initial slope of the  $\tau$  versus  $\gamma$  response and we take the shear strength of the material to be given as  $\tau_{31s} = \sigma_c/2$ , where  $\sigma_c$  is the peak measured values of

Property	Woven 0–90° orient.	Woven ±45° orient.	Laminate 0–90° orient.
$E_{1s} = E_{3s}$	63 GPa	16 GPa	65 GPa
$G_{31s}$	4.7 GPa	27 GPa	4.7 GPa
$\nu_{13s}$	0.16	0.70	0.10
$\sigma_c$	331 MPa	80 MPa	356 MPa
$\tau_{31s}$	40 MPa	166 MPa	45 MPa
$\rho$	1370 kgm <sup>-3</sup>		1590 kgm <sup>-3</sup>

**Table 2.** Measured material properties of the woven and laminate composite materials.

$\sigma_x$ . Similar procedures are followed to determine the shear properties of the woven material in the ±45° orientation and the laminate in the 0–90° orientation. These shear properties are also listed in Table 2.

**4.4. Comparison of measurements and predictions.** Predicted values of the moduli and peak strengths of the square honeycombs are included as continuous lines in Figures 12–15 for compressive loading and in Figure 18 for shear loading. Reasonable agreement is observed between measurements and predictions of the moduli and strength in the ±45° orientation for compression and 0–90° orientation for shear. By contrast, the analytical models over-predict the moduli and strengths of the honeycombs in the 0–90° and ±45° orientations for compression and shear, respectively. These results indicate that when the deformation of the honeycombs is primarily governed by the deformation of the matrix in the composite materials the models give reasonable predictions, while when fibre deformation is the primary deformation mode the analytical models significantly over-predict the measurements. We rationalise this by recalling that the compression of fibre composites along the fibre direction is very imperfection sensitive. An imperfection such as wavy cell walls results in a reduction in strength and stiffness of the honeycomb for two reasons: a geometric effect that induces bending moments in the cell walls, and an additional misalignment of the fibres with respect to the loading direction. The geometric effect is investigated by a limited finite element (FE) investigation reported in the Appendix but the effect of fibre misalignment is not included in the continuum cell wall models analysed here but can be summarised as follows. The microbuckling strength  $\sigma_c$  of composite is given as [Rosen 1965; Argon 1972; Budiansky 1983]

$$\sigma_c = \frac{k}{\bar{\phi}} \tag{18}$$

in terms of the matrix shear strength  $k$  and misalignment angle  $\bar{\phi}$  between the fibres and loading direction. The misalignment angle  $\bar{\phi}$  in case of the honeycombs has two contributions; the initial misalignment of the fibres in the laminate and the additional misalignment caused by the wavy cell walls of the honeycomb.

**5. Comparison with competing metallic cellular sandwich cores**

The performance of the composite square-honeycombs is compared with that of metallic sandwich cores in Figure 20, which includes data for stainless steel pyramidal cores [Côté et al. 2007], diamond cores and

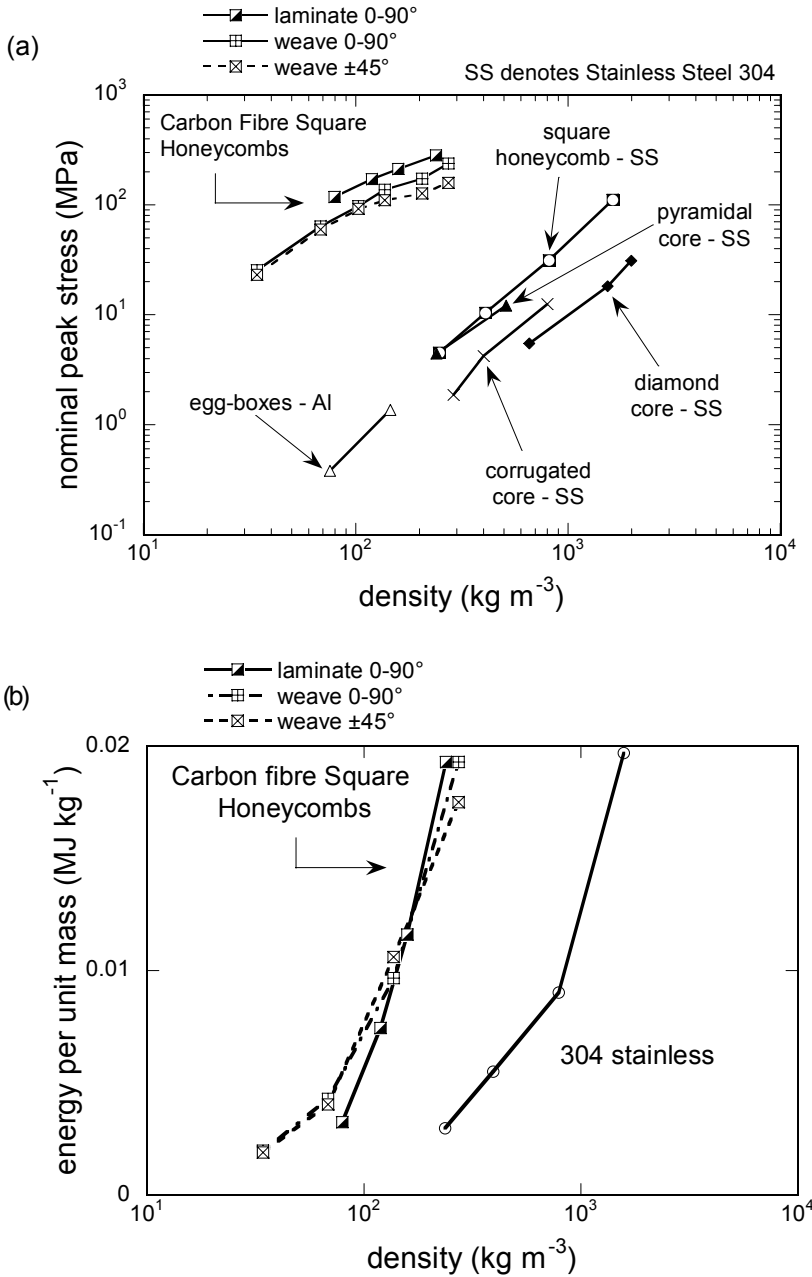


**Figure 20.** A comparison between the measured (a) peak compressive strengths  $\sigma_p$  and (b) energy absorption capacities per unit mass (up to a compressive strain  $\bar{\epsilon} = 0.4$ ) of competing metallic and composite sandwich cores as a function of the density  $\rho \equiv \bar{\rho}\rho_s$ .

corrugated cores [Côté et al. 2006] as well as aluminium egg-boxes [Zupan et al. 2003]. This comparison is presented for the compressive peak strength in Figure 20a and the compressive energy absorption per unit mass  $W_v/\rho$  up to a strain  $\bar{\epsilon} = 0.4$  in Figure 20b. For a given core density  $\rho \equiv \bar{\rho}\rho_s$ , where  $\rho_s$  is the density of the solid cell wall material, the composite square honeycombs outperform metallic cores both in terms of their peak strength and energy absorption capacity. More significantly, the composite materials appear to lie in an area of material space where metallic materials do not seem to exist at all.

To further explore the potential of composite cellular materials, consider the Ashby material property chart [Ashby and Bréchet 2003] shown in Figure 1. Aluminium foams and lattices occupy the low density region of material strength – density space. It also reveals a gap between the strength of existing lattice materials and the unattainable materials limit. The compressive strengths of composite honeycombs measured in the current study are included in Figure 1 and clearly show that cellular composite materials explored here reside in the gap in the material strength versus density space. Also included in Figure 1 is the theoretical prediction of the compressive strength of the 0–90° laminate (solid line). It is clear that topologically structuring composite materials in configurations such as the square honeycomb show promise for filling gaps in the strength versus density map of all known materials; the challenge is found in manufacturing these materials with minimum imperfections so as to attain their ideal strengths.

## 6. Concluding remarks

A preliminary investigation of the mechanical properties of square-honeycomb sandwich structures manufactured from carbon fibre reinforced polymers has been conducted. Honeycomb cores with relative densities  $\bar{\rho}$  in the range 2.5% to 20% were manufactured by slotting, assembling and adhesively bonding composite sheets. Their out-of-plan compressive and shear response are measured as a function of relative density, ratio of the specimen height to cell width, and number of cells in the specimen. The effect of the composite material type (laminate and woven) and material orientation on the compressive and shear responses of the honeycombs is also reported. The measurements indicate that the response is relatively insensitive to the ratio of the specimen height to cell width and number of cells in the specimen, but strongly dependent on the material type and orientation. In particular, the compressive strength of the honeycombs made from laminates with fibres aligned with the compression direction (i.e., 0–90° honeycombs) was greater than that of the honeycombs made from the woven material with fibres at  $\pm 45^\circ$  with respect to the compression direction. However, the energy absorption capacities of these two types of honeycombs were almost equal. The role of material orientation reversed for shear loading with the shear strength of the  $\pm 45^\circ$  honeycombs exceeding that of the 0–90° honeycombs.

In compression the honeycombs failed by either elastic buckling or plastic microbuckling while in shear the two main failure modes were elastic buckling or shear failure of the composite sheet material. Analytical models are derived for both collapse modes. The predicted strengths are substantially higher than the measurements especially when fibre deformation dominates the deformation of the composite sheets. These discrepancies result from imperfections arising in the manufacturing of the honeycombs and not accounted for in the analytical models. A limited finite element investigation quantified the significant effects of geometric imperfections on the compressive strength of the composite honeycombs.

The measurements and predictions reported here indicate that composite cellular materials with a square honeycomb topology reside in a gap in the strength versus density material property space, providing new opportunities for lightweight, high strength structural design.

**Appendix A. Finite element calculations of the compressive response of the square honeycombs**

The measured values of the peak strengths of the composite honeycombs are substantially below the analytical predictions. We have attributed this discrepancy to the presence of imperfections in the manufactured honeycombs that are not accounted for in the analytical model. In this Appendix we report a limited set of finite element (FE) calculations in order to gauge the effect of geometrical imperfections on the compressive response of the honeycombs.

**A1. Details of the FE calculations.** Finite deformation FE calculations were performed using the standard version of the commercial FE package ABAQUS (version 6.5). Calculations were performed on the honeycomb specimens comprising  $6 \times 6$  cells with a cell aspect ratio  $H/L = 3$  and made from the  $0-90^\circ$  woven material. In the honeycombs used in the experiments, cell wall thickness  $t$  was kept constant whilst varying the cell size  $L$ . However, in the FE model the cell size of the honeycombs was fixed at  $L = 10$  mm and the relative density varied by changing the cell wall thickness  $t$ . The honeycomb were discretised using 8-noded shell elements with reduced integration (S8R in the ABAQUS notation) with 5 integration points across the shell thickness. In all the calculations presented here square elements of length  $L/10 = 1$  mm were employed; further mesh refinements gave no appreciable change to the results reported. The FE model assumed perfect bonding along the cell edges and so did not account for the slotting and gluing procedure employed to manufacture the honeycombs. In all the calculations presented here geometrical imperfections were introduced into the FE model in the form of the eigen-mode shown in Figure 21a. This eigen-mode is in close agreement with the observed elastic collapse mode (Figure 8) and that of the analytical model. The magnitude of the imperfections is characterized by the maximum amplitude of the displacements of the cell walls from their original configuration: for each

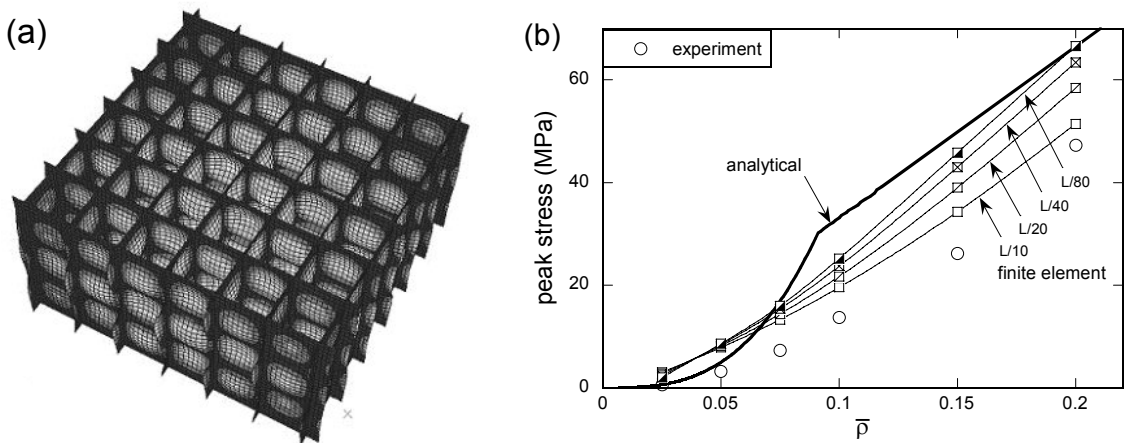


**Figure 21.** (a) The eigen-mode used to introduce geometrical imperfections in the FE models. (b) Comparison of the FE predictions and measured values of the peak compressive strengths of the honeycombs. FE predictions for 4 selected values of the imperfection magnitude are included along with the analytical predictions. All results are for the honeycombs made from the  $0 - 90^\circ$  woven material with  $6 \times 6$  cells and a cell aspect ratio  $H/L = 3$ .

value of the relative density  $\bar{\rho}$ , we shall report calculations with imperfection amplitudes  $L/10$ ,  $L/20$ ,  $L/40$  and  $L/80$ .

The top and bottom surfaces of the honeycomb were tied to two rigid surfaces with all degrees of freedom of the bottom surface constrained. A displacement rate  $\dot{\delta} = 0.002 \text{ ms}^{-1}$  in the  $x_3$  direction was applied to the top surface with displacements of that surface in the  $x_1$  and  $x_2$  directions prevented. The applied stress on the honeycomb was inferred from the work conjugate force to the applied displacement in the  $x_3$  direction.

Unless otherwise specified, the cell wall material was modelled as an elastic-plastic solid. While the elastic response was assumed to be orthotropic (elastic properties listed in Table 2) for the 0–90° woven composite, the failure of the composite material under compression was assumed to be approximately captured by a nonhardening J2 flow theory plastic response with a yield strength given by the compressive strength  $\sigma_c$  listed in Table 2.

**A2. Summary of findings.** The FE predictions of the compressive peak strength of the honeycombs are plotted in Figure 21b as a function of  $\bar{\rho}$  for selected values of the imperfection magnitude. The measured values of the peak strengths and the corresponding analytical predictions are also included in Figure 21b. We observe that the imperfections not only significantly reduce the peak strengths of the honeycombs but also affect the form of the variation of the peak strength  $\sigma_p$  with relative density  $\bar{\rho}$  when compared with the analytical predictions. Reasonable agreement between the measurements and FE predictions, especially at high values of  $\bar{\rho}$ , is observed for the largest imperfection magnitude of  $L/10$ .

Recall that under compression, the composite displays a strongly softening response; while in the FE results presented in Figure 21b, the material was assumed to be ideally plastic. In order to explore the validity of the material model, we conducted some additional FE calculations with the material described by a softening post-yield material response as sketched in Figure 22a. In particular the material was assumed to be orthotropic elastic up to the yield strength  $\sigma_c$ . Subsequently the material was again assumed as a J2 flow theory material but with a linearly softening post-yield response. The softening rate in terms of the uniaxial stress versus strain response was assumed  $-d\sigma/d\varepsilon = 0.5E_{3s}$ . FE predictions of the peak strengths with this new material model are plotted in Figure 22b (for an imperfection magnitude  $L/10$ ) along with the corresponding FE calculations assuming nonhardening plasticity from Figure 21b and the experimental measurements. Including the softening post-yield response of the composite material appears to have a negligible effect on the peak strength of the honeycombs and thus suggesting that a nonhardening plasticity model is an adequate representation of the composite material in terms of modelling the peak strength of the honeycombs.

In addition to the FE calculations presented here, we also performed the following FE calculations in order to further explore the origins of the rather low measured strengths of the honeycombs:

- (i) In order to investigate the effect of loading asymmetry in the experiments, a loading rate  $\dot{\delta} + \omega x_2$  was imposed on the top rigid surface with the rotation rate  $\omega = 0.03 \text{ rad s}^{-1}$ . This had a negligible effect on the predicted peak strengths.
- (ii) Recall that the honeycombs were manufactured by slotting together sheets and gluing the assembly. The effect of this manufacturing process was modelled in the FE calculations by detaching the cells walls along half the height of the honeycomb (using the “seams” option in ABAQUS). FE predictions using this model gave results very similar to those presented in Figure 22b.

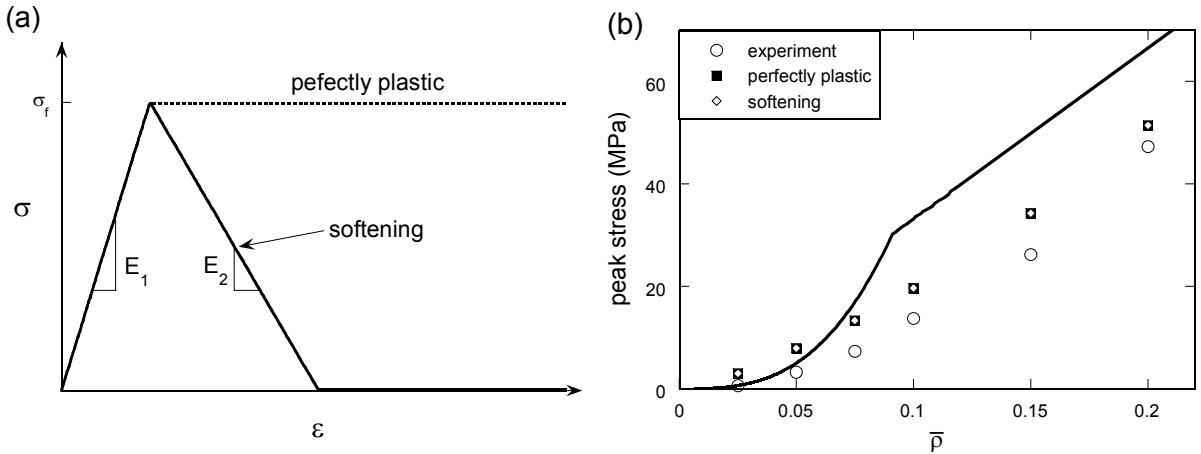


**Figure 22.** (a) Sketch of the nonhardening and softening uniaxial stress versus strain responses employed to model the solid composite material in the FE calculations. (b) Comparison of the FE predictions of the peak compressive strengths of the honeycombs with measurements. FE predictions for the nonhardening and softening material models with an imperfection magnitude  $L/10$  are included along with the analytical predictions. All results are for the honeycombs made from the  $0\text{--}90^\circ$  woven material with  $6 \times 6$  cells and a cell aspect ratio  $H/L = 3$ .

We conclude that imperfections in terms of wavy cell walls seem to be the main source of the discrepancy between the measured values and analytical predictions of the peak strength of the composite honeycombs, of which both geometrical effects and fibre misalignment effects contribute to the reduction in peak stress.

### Acknowledgements

We are grateful to the Office of Naval Research (ONR) for the funding of this project under grant number N00014-01-1-1051, with Dr. David Shifler as program manager.

### References

- [Argon 1972] A. S. Argon, “Fracture of composites”, *Treatise Mater. Sci. Technol.* **1** (1972), 79–114.
- [Ashby and Bréchet 2003] M. F. Ashby and Y. J. M. Bréchet, “Designing hybrid materials”, *Acta Mater.* **51**:19 (2003), 5801–5821.
- [Ashby et al. 2000] M. F. Ashby, A. G. Evans, N. A. Fleck, L. J. Gibson, J. W. Hutchinson, and H. N. G. Wadley, *Metal foams: a design guide*, Butterworth-Heinemann, Boston MA, 2000.
- [ASTM 2000] ASTM, “Test method for shear properties of Sandwich core materials”, 2000. Volume 15.03.
- [Budiansky 1983] B. Budiansky, “Micromechanics”, *Comput. Struct.* **16** (1983), 3–12.
- [Côté et al. 2004] F. Côté, V. S. Deshpande, N. A. Fleck, and A. G. Evans, “The out-of-plane compressive behavior of metallic honeycombs”, *Mater. Sci. Eng. A* **380**:1–2 (2004), 272–280.
- [Côté et al. 2006] F. Côté, V. S. Deshpande, N. A. Fleck, and A. G. Evans, “The compressive and shear responses of corrugated and diamond lattice materials”, *Int. J. Solids Struct.* **43**:20 (2006), 6220–6242.

- [Côté et al. 2007] F. Côté, N. A. Fleck, and V. S. Deshpande, “Fatigue performance of sandwich beams with a pyramidal core”, *Int. J. Fatigue* **29**:8 (2007), 1402–1412.
- [Deshpande et al. 2001a] V. S. Deshpande, M. F. Ashby, and N. A. Fleck, “Foam topology: bending versus stretching dominated architectures”, *Acta Mater.* **49**:6 (2001), 1035–1040.
- [Deshpande et al. 2001b] V. S. Deshpande, N. A. Fleck, and M. F. Ashby, “Effective properties of the octet-truss lattice material”, *J. Mech. Phys. Solids* **49**:8 (2001), 1747–1769.
- [Ericksen and March 1958] W. S. Ericksen and H. W. March, “Compressive buckling of sandwich panels having dissimilar facings of unequal thickness”, Report 1583-B, Forest Products Laboratory, Madison, WI, 1958.
- [Evans et al. 1998] A. G. Evans, J. W. Hutchinson, and M. F. Ashby, “Multifunctionality of cellular metal systems”, *Prog. Mater. Sci.* **43**:3 (1998), 171–221.
- [Finnegan et al. 2007] K. Finnegan, G. Kooistra, H. N. G. Wadley, and V. S. Deshpande, “The compressive response of carbon fiber composite pyramidal truss sandwich cores”, *Int. J. Mater.* (2007), 1264–1272.
- [Fleck and Deshpande 2004] N. A. Fleck and V. S. Deshpande, “The resistance of clamped sandwich beams to shock loading”, *ASME J. Appl. Mech.* **71** (2004), 386–401.
- [Gibson and Ashby 1997] L. J. Gibson and M. F. Ashby, *Cellular solids, structure and properties*, 2nd ed., Cambridge University Press, Cambridge, 1997.
- [Krivetsky 1959] A. Krivetsky, “Buckling of orthotropic plates (corrugated plate applications)”, Report 7-60-941001, Bell Aerospace Company, 1959.
- [Marasco et al. 2006] A. I. Marasco, D. D. R. Cartié, I. K. Partridge, and A. Rezaei, “Mechanical properties balance in novel Z-pinned sandwich panels: Out-of-plane properties”, *Compos. A: Appl. Sci. Manuf.* **37**:2 (2006), 295–302.
- [Rosen 1965] B. W. Rosen, “Mechanics of composite strengthening”, Chapter 3, pp. 37–75 in *Fiber composite materials*, American Society for Metals, Metals Park, OH, 1965.
- [Seydel 1930] E. Seydel, “Jahrbuch 1930 der Deutschen Versuchsanstalt für Luftfahrt”, NACA Technical Memorandum 602, 1930.
- [Wadley 2002] H. N. G. Wadley, “Cellular materials manufacturing”, *Advanced Eng. Mat.* **4**:10 (2002), 726–733.
- [Wadley 2006] H. N. G. Wadley, “Multifunctional periodic cellular metals”, *Phil. Trans. R. Soc. A* **364** (2006), 31–68.
- [Xue and Hutchinson 2004] Z. Xue and J. W. Hutchinson, “A comparative study of impulse-resistant metal sandwich plates”, *Int. J. Impact Eng.* **30**:10 (2004), 1283–1305.
- [Zupan et al. 2003] M. Zupan, C. Chen, and N. A. Fleck, “The plastic collapse and energy absorption capacity of egg-box panels”, *Int. J. Mech. Sci.* **45**:5 (2003), 851–871.

Received 21 Feb 2008. Revised 23 May 2008. Accepted 1 Jun 2008.

BENJAMIN P. RUSSELL: bpr23@cam.ac.uk  
Engineering Department, Trumpington Street, University of Cambridge, Cambridge CB2 1PZ, United Kingdom

VIKRAM S. DESHPANDE: vsd@engineering.ucsb.edu  
Engineering Department, Trumpington Street, University of Cambridge, Cambridge CB2 1PZ, United Kingdom

HAYDN N. G. WADLEY: haydn@virginia.edu  
Department of Materials Science and Engineering, University of Virginia, 395 McCormick Road, Charlottesville VA 22904, USA